# Electron-impact excitation-autoionization in the cadmium isoelectronic sequence: A case of target term dependence in scattering theory

M. S. Pindzola
*Department of Physics, Auburn University, Auburn, Alabama 36849*
*and Physics Division, Oak Ridge National Laboratory, Oak Ridge, Tennessee 37830*

D. C. Griffin
*Department of Physics, Rollins College, Winter Park, Florida 32789*
*and Physics Division, Oak Ridge National Laboratory, Oak Ridge, Tennessee 37830*

C. Bottcher
*Physics Division, Oak Ridge National Laboratory, Oak Ridge, Tennessee 37830*
(Received 20 September 1982)

Excitation-autoionization contributions to electron-impact ionization are calculated for several atomic ions in the cadmium isoelectronic sequence. We calculate excitation cross sections in the distorted-wave approximation and compare them in one case to a calculation in the close-coupling approximation. We focus attention on the $4d^{10}5s^2 \rightarrow 4d^9 5s^2 nf$ inner-shell excitations in $In^+$, $Sb^{3+}$, and $Xe^{6+}$. Hartree-Fock atomic structure calculations for the $4d^9 5s^2 nf$ configurations are found to be highly term dependent. Thus our predictions for the total ionization cross section from the $5s$ subshell for these ions exhibit strong target term dependence. Our $Xe^{6+}$ results are found to be in excellent agreement with the recent experimental crossed-beam measurements of Gregory and Crandall.

## I. INTRODUCTION

The interpretation of resonances in electron-atomic ion scattering experiments tests our theoretical understanding of both atomic structure and collision dynamics. As recently emphasized,[1] large staircaselike resonance structures may occur in the electron-impact ionization of heavy atoms in low stages of ionization. The resonance mechanism is the inner-shell excitation of a bound level lying above the ionization limit, followed by autoionization. Typical Lorentzian resonance profiles will then occur in the differential cross section in the ejected-electron energy, which upon integration yields a series of steps in the total ionization cross section. These core-excited autoionization states in neutral atoms have been studied for many years in both high-resolution electron spectroscopy and photoionization experiments.[2]

Owing to its closed-shell nature ($4d^{10}5s^2$), and thus its simple atomic level structure, the cadmium isoelectronic sequence is quite suitable for making a detailed theoretical investigation of excitation-autoionization contributions to electron-impact ionization. The ejected-electron[3] and photoelectron[4] spectrums of neutral Cd reveal many resonance structures. It is interesting to track just the $4d^{10}5s^2 \rightarrow 4d^9 5s^2 4f$ transitions along the cadmium isoelectronic sequence to see if at some ionization stage they make large contributions to the ionization cross section. In moving along the isoelectronic sequence, term-dependent atomic structure effects in the ionization cross section should appear in a manner similar to those found in line strength calculations for the $4d^{10} \rightarrow 4d^9 4f$ transition in the palladium isoelectronic sequence.[5] Term-dependent effects in energy-level structures and on various atomic parameters have been reported by a number of authors.[6–9]

In Sec. II of this paper we analyze, through the calculation of an effective potential, term-dependent effects in the $4d^{10}5s^2 \rightarrow 4d^9 5s^2 4f$ inner-shell excitations of $In^+$, $Sb^{3+}$, and $Xe^{6+}$. In Sec. III we outline in detail our calculation of the $4d^9 5s^2 4f\,{}^1P_1$ excitation-autoionization contribution to the ionization of $Xe^{6+}$ using both the close-coupling and distorted-wave approximations. In Sec. IV we present and discuss our intermediate-coupled, distorted-wave approximation results for $In^+$, $Sb^{3+}$, and $Xe^{6+}$. We also compare our $Xe^{6+}$ calculation with the recent experimental crossed-beam measurements of Gregory and Crandall.[10] Section V contains a brief summary.

## II. ATOMIC STRUCTURE CALCULATIONS

We made Hartree-Fock atomic structure calculations for several atomic ions in the cadmium

 

isoelectronic sequence. Term-dependent effects in energy-level structures and on various atomic parameters are particularly pronounced in the configuration $4d^9 5s^2 4f$. To understand this we must consider the expressions for the energies of particular $LS$ terms in such a configuration and in the form of the effective central potential that the outer electron in such a configuration experiences. The energy of the $^1P$ term, $E(^1P)$, ignoring spin-orbit interactions, is given by the expression

$$E(^1P)=E(\mathrm{CA})-\frac{8}{35}F^2(df)-\frac{2}{21}F^4(df)+\frac{137}{70}G^1(df)-\frac{2}{105}G^3(df)-\frac{5}{231}G^5(df), \quad (1)$$

where $E(\mathrm{CA})$ is the configuration-average energy, $F^\kappa$ is the direct electrostatic radial integral, and $G^\kappa$ is the exchange electrostatic radial integral.[11] We note the large positive angular coefficient for the $G^1(df)$ integral. The energies of the nine remaining $LS$ terms are close to the configuration-averaged energy. The large positive coefficient of $G^1(df)$ may cause the $^1P$ term to occur well above the positions of the other $LS$ terms. A $^1P$ term-dependent Hartree-Fock calculation may thus produce direct potentials, exchange functions, and radial wave functions which vary significantly from those obtained in a configuration-average Hartree-Fock calculation.

As a guide in studying term-dependent effects, it is useful to introduce the effective central potential, which for the Hartree-Fock equations is given by

$$V_{\mathrm{eff}}(r)=\frac{l(l+1)}{r^2}-\frac{2Z}{r}+\frac{2}{r}Y(n,l;r)+\frac{2}{r}\frac{X(n,l;r)}{P_{nl}(r)}+\sum_{n'}\frac{\epsilon_{nl,n'l}P_{n'l}(r)}{P_{nl}(r)}, \quad (2)$$

where we use a notation similar to Fischer's.[12] In Eq. (2), $Z$ is the atomic number, $2Y(n,l;r)/r$ is the direct potential, $2X(n,l;r)/r$ is the exchange function, and $\epsilon_{nl,n'l}$ is a Lagrangian multiplier. We must emphasize that we only use the $V_{\mathrm{eff}}(r)$ as a descriptive device for explaining wave-function collapse; all bound radial functions used in this paper are self-consistent solutions to the Hartree-Fock equations. The effective potential equation for a radial function may be written as

$$\left[-\frac{d^2}{dr^2}+V_{\mathrm{eff}}(r)\right]P_{nl}(r)=\epsilon_{nl}P_{nl}(r), \quad (3)$$

where $V_{\mathrm{eff}}(r)$ and $\epsilon_{nl}$ are in rydbergs. The effective potential in Eq. (2) is well defined for nodeless radial functions, such as $P_{4f}(r)$. In other cases a simple linear interpolation may be used so that singularities do not appear in graphical display. We modified Fischer's multiconfiguration Hartree-Fock computer code[13] to calculate $V_{\mathrm{eff}}(r)$ from Eq. (2). Effective potentials, using the Hartree-exchange approximation, were used to explain the $d$-electron collapse at the beginning of the transition series and the $f$-

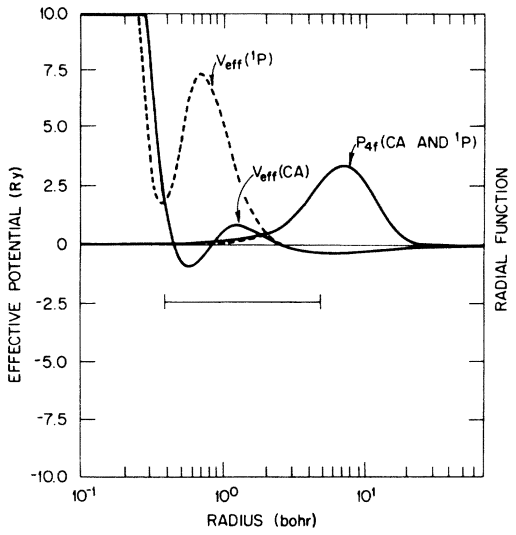


FIG. 1. Plot of the $4f$ [CA] (solid curves) and $4f[^1P]$ (dotted curves) effective potentials and radial functions for the $4d^9 5s^2 4f$ configuration in $In^+$. A logarithmic scale is used for the radius. The bar indicates the range of radii over which the second antinode of the $4d$ radial function occurs.

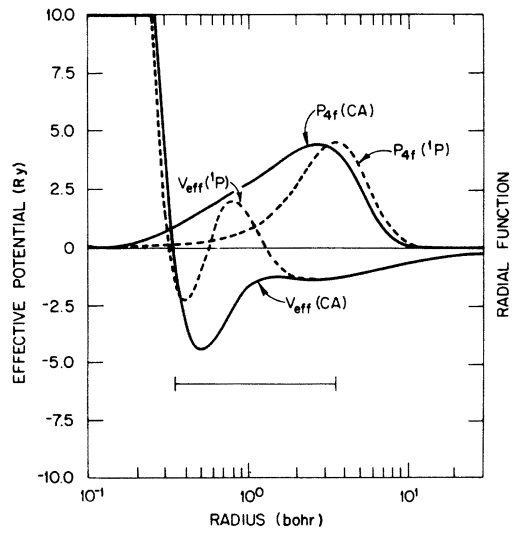


FIG. 2. Plot of the $4f$ [CA] (solid curves) and $4f[^1P]$ (dotted curves) effective potentials and radial functions for the $4d^9 5s^2 4f$ configuration in $Sb^{3+}$. A logarithmic scale is used for the radius. The bar indicates the range of radii over which the second antinode of the $4d$ radial function occurs.

electron collapse at the beginning of the rare-earth series[14] following the classical work of Mayer,[15] who used Thomas-Fermi potentials to predict the onset of the rare-earth series. Effective potentials have also been used to provide insight into the construction of atomic pseudopotentials for metallic band-structure calculations.[16]

As seen in Figs. 1–3, both configuration-average and $^1P$ term-dependent Hartree-Fock effective potentials for the $4f$ radial function in the $4d^95s^24f$ configuration may have pronounced double-well structures along the cadmium isoelectronic sequence. In Fig. 1 for $In^+$, the effective potential for the $^1P$ term (because of the positive exchange contribution arising from the $G^1$ integral) has both a large positive barrier and a positive inner well, while for the other terms, approximated by the configuration-average potential, the barrier is small and the inner well is negative. Nevertheless the configuration-average $4f$[CA] radial function and the $^1P$ term-dependent $4f[^1P]$ radial function are almost identical and lie in the outer potential region where they are essentially $4f$ hydrogenic wave functions. In Fig. 2. for $Sb^{3+}$, the increase in the nuclear charge causes the potential barrier for the configuration-average effective potential to become negative and nearly disappear, while the $4f$ [CA] radial function collapses into the inner-well region. Meanwhile, the barrier for the $^1P$ effective potential remains positive and large enough to keep the $4f[^1P]$ radial function in the outer-well region. The difference in the two radial functions is reflected in their values for the radial dipole-matrix element with the $4d$ radial function. For the $4f$ [CA], $\langle 4d \mid r \mid 4f \rangle = -0.644a_0$, while for the $4f[^1P]$, $\langle 4d \mid r \mid 4f \rangle = -0.343a_0$, where $a_0$ is the Bohr radius. In Fig. 3 for $Xe^{6+}$, the further increase in the nuclear charge has caused the potential barrier for the $^1P$ effective potential to become negative and small, and the $4f[^1P]$ radial function is on the verge of collapsing into the inner-well region. For the $4f$ [CA], $\langle 4d \mid r \mid 4f \rangle = -0.874a_o$, while for the $4f[^1P]$, $\langle 4d \mid r \mid 4f \rangle = -0.676a_0$. For high stages of ionization the potential barrier becomes insignificant for the $^1P$ effective potential and the $4f[^1P]$ radial function collapses into the inner potential region where the two radial functions are again almost identical but nonhydrogenic.

In $In^+$ and $Sb^{3+}$ the 20 $LSJ$ levels of the $4d^95s^2$ configuration all lie above the $4d^{10}5s$ ionization limit as shown in Fig. 4. Thus they contribute through excitation-autoionization to the electron-impact ionization of these ions at incident energies near threshold. As will be discussed in Sec. IV, the term-dependent effects found in analyzing the $Sb^{3+}$ radial functions lead us to predict an unusual shape in the total ionization cross section. In $Xe^{6+}$ only the $^1P_1$ level is autoionizing, while the remaining levels in the $4d^95s^24f$ configuration are true bound states as shown in Fig. 4. In Secs. III and IV, we find that term-dependent effects in $Xe^{6+}$ not only affect the

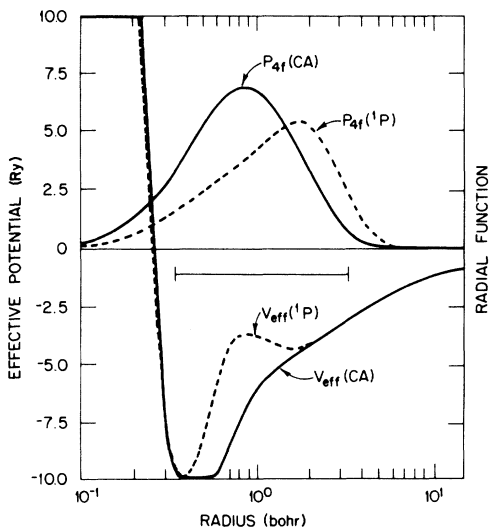


FIG. 3. Plot of the $4f$ [CA] (solid curves) and $4f[^1P]$ (dotted curves) effective potentials and radial functions for the $4d^95s^24f$ configuration in $Xe^{6+}$. A logarithmic scale is used for the radius. The bar indicates the range of radii over which the second antinode of the $4d$ radial function occurs.

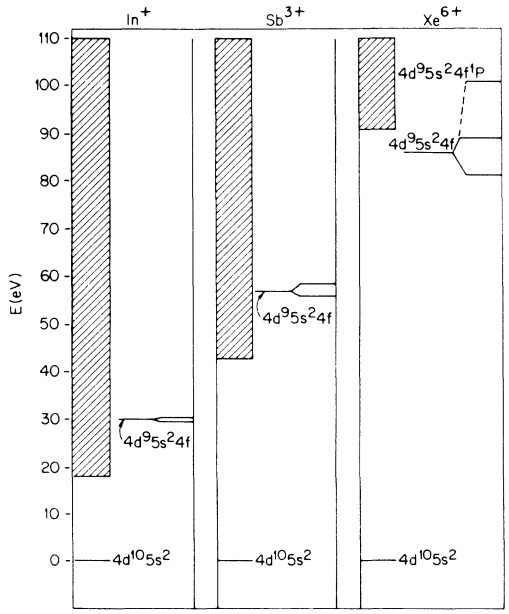


FIG. 4. Energy-level diagrams showing the $4d^95s^24f$ configurations of $In^+$, $Sb^{3+}$, and $Xe^{6+}$ with respect to the ionization thresholds. Hatched region indicates the ionization continuum for the next-higher ionization stage.

TABLE I. $Xe^{6+}$ energies (in eV).

| Method | Ionization potential | $4d^9 5s^2 4f$ configuration-average | $4d^9 5s^2 4f\ ^1P_1$ |
|---|---|---|---|
| Hartree-Fock (HF) | 86.6 | 85.4 | 100.8 |
| Hartree-Fock relativistic (HFR) | 89.6 | 84.7 | 99.1 |
| Hartree-Fock relativistic with 5*s* pair correlations (HFR*s*) | 90.7 | 84.7 | 99.1 |
| Hartree-Fock relativistic with 5*s* and 4*d* pair correlations (HFR*sd*) | 90.7 | 86.0 | 100.4 |

spectrum of possible autoionizing levels, but the magnitudes of excitation-autoionization contributions as well.

## III. CLOSE-COUPLING CALCULATION FOR Xe VII

We calculated excitation-autoionization contributions to the electron-impact ionization of $Xe^{6+}$ in both the close-coupling and distorted-wave approximations. An intermediate-coupling calculation, described in Sec. IV, shows that the $4d^9 5s^2 4f\ ^1P_1$ resonance level is over 99% pure. However, most of the 19 lower bound levels of the $4d^9 5s^2 4f$ configuration show large spin-orbit mixing effects. We will thus treat the $^1P_1$ level as a single *LS* term in the calculations described in this section.

In calculating the contributions of excitation autoionization for $Xe^{6+}$, it is important to obtain the energies of the quasibound states accurately. Our single-configuration Hartree-Fock (HF) values of the ionization potential, the configuration-average energy of the $4d^9 5s^2 4f$, and the energy of the $4d^9 5s^2 4f\ ^1P_1$ are given in the first row of Table I. The energies in Table I are obtained by taking differences between single-configuration HF calculations. We also included relativistic effects by using the Hartree-Fock method with relativistic modifications (HFR), which allows for the mass velocity and Darwin corrections within modified HF differential equations.[17] As given in Table I, sizable relativistic effects for the 5*s* radial function raise the ionization potential by 3.0 eV. Relativistic effects lower the energy of the $4d^9 5s^2 4f$ configuration due to the reduction in shielding when a 4*d* electron is promoted to a 4*f* subshell. This shift is larger for the $4d^9 5s^2 4f\ ^1P_1$ level because the 4*f* electron in the $^1P$ state provides even less shielding.

We found the effects of electron correlation to be moderately important for $Xe^{6+}$. We included 5*s* pair correlation in the ground state by performing a multiconfiguration Hartree-Fock (MCHF) calculation[13] for $4d^{10} 5s^2$ plus $4d^{10} 5p^2$. If we assume that 5*s* pair correlation is the same in $4d^9 5s^2 4f$, this effect increases the ionization potential by 1.1 eV, but does not affect the position of the $4d^9 5s^2 4f$ configuration. This estimate is designated by HFR*s* in Table I. We also included 4*d* pair correlation in the ground state by performing an MCHF calculation for $4d^{10} 5s^2$ plus $4d^8 4f^2 5s^2$. The total pair correlation energy within the $4d^{10}$ subshell is 6.4 eV. By taking the difference between the number of 4*d* pairs, we obtain a correction of 1.3 eV for the energy difference between the $4d^{10} 5s^2$ and $4d^9 5s^2 4f$ configurations. This estimate, which does not affect the ionization potential, is designated by HFR*sd* in Table I.

We first calculated the $4d^9 5s^2 4f\ ^1P_1$ electron-impact excitation cross section for $Xe^{6+}$ in the distorted-wave approximation. We included both direct and exchange matrix elements in a standard partial-wave expansion for the cross section.[18] To evaluate the radial matrix elements we used HF threshold energies, HF bound radial functions, and scattering orbitals calculated in the continuum HF approximation.[19] Both incoming and outgoing waves were calculated in the nonlocal distorting potential of the ground $4d^{10} 5s^2\ ^1S$ state in order to simplify orthogonality conditions. Our results obtained with the use of both configuration-average and term-dependent 4*f* radial functions, are shown in Fig. 5. We found a factor-of-2 reduction in the excitation cross section due to term dependence. As discussed in Sec. II the collapsed $4f$[CA] radial function has a much stronger overlap with the 4*d* than the $4f[^1P]$ radial function, which still resides at least partially in the outer well. To estimate the

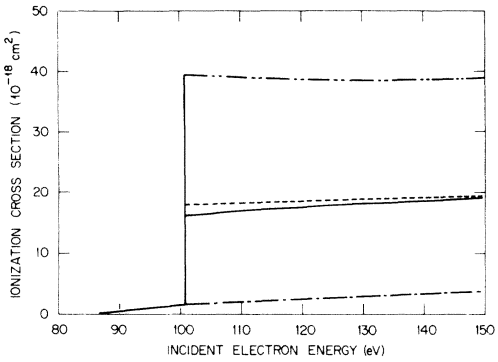


FIG. 5. Total ionization cross section for $Xe^{6+}$. Dot-dash curve, direct-ionization cross section calculated from the Lotz equation; solid curve, term-dependent close-coupling $4d^9 5s^2 4f\ ^1P_1$ excitation cross section plus Lotz; dotted curve, term-dependent distorted-wave $4d^9 5s^2 4f\ ^1P_1$ excitation cross section plus Lotz; chain curve, configuration-average distorted-wave $4d^9 5s^2 4f\ ^1P_1$ excitation cross section plus Lotz.

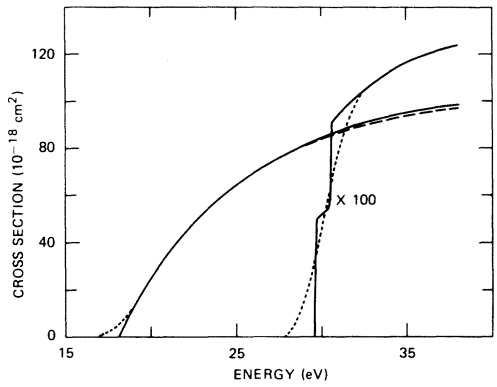


FIG. 6. Total ionization cross section for $In^+$. Dashed curve, direct-ionization cross section calculated from the Lotz equation; solid curve, intermediate-coupled distorted-wave excitation cross sections for $4d^{10}5s^2 \rightarrow 4d^9 5s^2 4f$ plus Lotz; dotted curve, solid curve convoluted with 2-eV-width Gaussian as a model of apparatus resolution. The indirect contribution is shown separately on a magnified scale.

direct-ionization cross section in Fig. 5 we used the semiempirical formula of Lotz.[20]

We also calculated the $4d^9 5s^2 4f\ ^1P_1$ excitation cross section for $Xe^{6+}$ in a two-state close-coupling approximation. We used our term-dependent radial orbitals as input to Seaton's IMPACT code.[21] As shown in Fig. 5 our close-coupling and distorted-wave results are in reasonable agreement. We note that if configuration-average radial orbitals are used in a close-coupling calculation, the results will also be high by a factor of 2.

For dipole-allowed excitation cross sections a simple method[22] can be used to estimate important correlation effects in the target. A single-configuration HF calculation for the $4d^{10}5s^2\ ^1S \rightarrow 4d^9 5s^2 4f\ ^1P$ oscillator strength yields a value 6.18 in the "length" gauge. If we include the $4d^8 4f^2 5s^2$ configuration in the ground state, an MCHF calculation drops the oscillator strength to $f=5.01$. We thus estimate a further 20% reduction in our term-dependent results in Fig. 5.

## IV. DISTORTED-WAVE CALCULATIONS FOR In II, Sb IV, AND Xe VII

We calculated excitation-autoionization contributions to the electron-impact ionization of $In^+$, $Sb^{3+}$, and $Xe^{6+}$ in the distorted-wave approximation modified for intermediate coupling. We used HFR*sd* threshold energies and HFR bound radial functions. The intermediate-coupled eigenvectors and energies were calculated using an atomic structure program furnished to us by Cowan.[23] A general collision algebra code developed by one of us (C. B.) was then used to form a list of direct and exchange matrix elements needed to determine the overall excitation cross section. The scattering orbitals needed to evaluate the radial matrix elements were calculated in a local distorting potential constructed in a semiclassical exchange approximation.[24] This exchange term simplifies the solution of the differential equations and gives results in close agreement with results obtained from the HF distorted-wave program. We again used the Lotz formula to provide an estimate for the direct-ionization cross section.

Our total electron-impact ionization cross-section results for $In^+$ are presented in Fig. 6. The direct

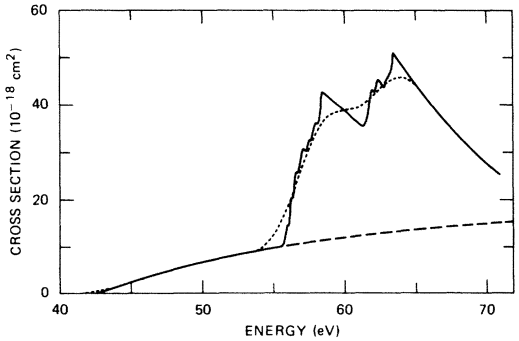


FIG. 7. Total ionization cross section for $Sb^{3+}$. Dashed curve, direct-ionization cross section calculated from the Lotz equation; solid curve, intermediate-coupled distorted-wave excitation cross sections for $4d^{10}5s^2 \rightarrow 4d^9 5s^2 nf (n=4,5)$ plus Lotz; dotted curve, solid curve convoluted with 2-eV-width Gaussian as a model of apparatus resolution.

knockout of the $5s$ electron dominates the near-threshold cross section. The excitation-autoionization contributions from the 20 levels associated with the $4d^9 5s^2 4f$ configuration appear as only a very small step around 30 eV incident electron energy. This can be explained in part by the hydrogenic nature of the $4f$ radial function and its subsequent small overlap with the $4d$.

In Fig. 7 we present electron-impact ionization cross sections for $Sb^{3+}$. In comparison with $In^+$ the excitation-autoionization contributions for $Sb^{3+}$ are quite sizable. This can be explained in part by the collapse of the $4f$ [CA] radial function, which results in large excitation cross sections to the lower levels of the $4d^9 5s^2 4f$ configuration. The most peculiar feature in Fig. 7 is the rapid drop in the cross section after the excitation of the $4d^9 5s^2 4f\ ^1P_1$ level at 58.1 eV, which also can be explained in terms of the term-dependent effects discussed in Sec. II. In most cases excitations to a dipole-allowed level, such as the $4d^9 5s^2 4f\ ^1P_1$, will dominate the spectrum of excitations found in a particular configuration. The total excitation cross section to the configuration will then fall off quite slowly with energy. For $Sb^{3+}$, however, the fact that the $4f[^1P]$ radial function still remains in the outer potential well will substantially reduce the $^1P_1$ excitation-autoionization contribution. Thus the many nondipole excitations, with their rapid falloff in energy, dominate the excitation spectrum. A recent electron-impact ionization experiment[25] on $Xe^{3+}$ ($4d^{10} 5s^2 5p^3$) shows a large hump in the cross section, which we believe to be due to a similar effect coming from excitations to the $4d^9 5s^2 5p^3 4f$ configuration.

Excitation-autoionization contributions from the $4d^9 5s^2 5f$ configuration appear in Fig. 7 for $Sb^{3+}$ at around 63 eV. As one would expect, the $5f$ excitation contributions are smaller than those from the $4f$ due to the extra node and the larger radial extent of the $5f$ radial function as compared to the $4f$. Term-dependent effects still play a strong role in the determination of the $4d^9 5s^2 5f$ configuration cross sections. In a manner similar to the $4f$, the $5f$ [CA] radial function overlaps more strongly with the $4d$ than does the $5f[^1P_1]$. The many nondipole transitions dominate the excitation spectrum and the unusual shape of the $4f$ excitations is repeated at higher energies for the $5f$ excitations. In atomic structure parlance we have observed the transfer of oscillator strength of both the $4f$ and the $5f$ to higher members of the Rydberg sequence; and perhaps into the continuum as observed in photoionization studies of neutral Ba.[26]

Our more complete electron-impact ionization results for $Xe^{6+}$ are presented in Fig. 8 along with the recent experimental measurements of Gregory and Crandall.[10] The overall agreement between theory and experiment is excellent. As explained in earlier sections the $^1P_1$ level at 100.4 eV is the only autoionizing state in the $4d^9 5s^2 4f$ configuration. We see in Fig. 8 that the $4f\ ^1P_1$ level makes the largest single-excitation-autoionization contribution to the cross section. As emphasized in Sec. III a term-dependent $4f[^1P]$ radial function must be used in the excitation cross-section calculation. The curve labeled $O$ (for optical) in Fig. 8 is the total excitation cross section to the 19 nonautoionizing levels of the $4d^9 5s^2 4f$ configuration.

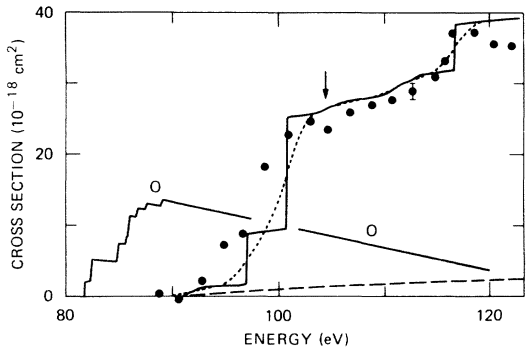


FIG. 8. Total ionization cross section for $Xe^{6+}$. Dashed curve, direct-ionization cross section calculated from the Lotz equation; solid curve, intermediate-coupled distorted-wave excitation cross sections for $4d^{10} 5s^2 \rightarrow 4d^9 5s^2 nf$ ($n=4,5$), $4d^9 5s^2 5d$, and $4d^9 5s^2 6p$ plus Lotz; dotted curve, solid curve convoluted with 2-eV-width Gaussian as a model of apparatus resolution; solid curve labeled $O$ (for optical) is the total excitation cross section to nonautoionizing levels of $4d^9 5s^2 4f$. $I$, experimental measurements (Ref. 10).

The steady rise in the cross section at around 112 eV in Fig. 8 is due to excitations to the lower levels of the $4d^9 5s^2 5f$ configuration. The step at 116.4 eV is excitation to the $4d^9 5s^2 5f\ ^1P_1$ level. Unlike $Sb^{3+}$, the $5f[^1P_1]$ radial function of $Xe^{6+}$ overlaps more strongly with the $4d$ than does the $5f$ [CA]. The increase in nuclear charge in going from $Sb^{3+}$ to $Xe^{6+}$ causes the first antinode in the $5f$ [CA] radial function to occur at a radius small enough to reduce its overlap with the second $4d$ antinode, while the first antinode in the $5f[^1P]$ radial function is nearly coincident with the second $4d$ antinode. Thus, contrary to the case of $Sb^{3+}$, some of the $4f$ oscillator strength has been transferred to the $5f$. The total excitation cross section to the configuration has the staircaselike appearance resulting from the slow falloff in energy of the strong dipole transition.

For $Xe^{6+}$ we also included excitation-autoionization contributions from the $4d^9 5s^2 5d$ and $4d^9 5s^2 6p$ configurations. Term-dependent effects in

these configurations are negligible and the only significant contribution to the ionization cross section came from the $4d^9 5s^2 5d\ ^1S_0$ level at 96.9 eV. This monopole-dominated transition should also be included in a more complete calculation for $Sb^{3+}$. The fact that theory is still a little above experiment in Fig. 8 suggests that electron correlation effects in the target, as discussed in Sec. III, may account for the remaining differences.

## V. SUMMARY

In conclusion we have found that excitation-autoionization contributions to the electron-impact ionization of atomic ions in the cadmium isoelectronic sequence may be quite significant. Atomic structure effects dominate the calculation of excitation cross sections for these heavy atomic systems. The differences between close-coupling and distorted-wave collisional methods are small compared to differences found between results obtained with the use of configuration-average and term-dependent core orbitals. From this and earlier work we must conclude that no simple isoelectronic scaling laws for the indirect cross section in complex atomic ions will exist.

## ACKNOWLEDGMENTS

We wish to thank R. D. Cowan for making his atomic structure program available to us and to acknowledge C. F. Fischer, S. M. Younger, H. E. Saraph, D. C. Gregory, and D. H. Crandall for a number of useful conversations. This work was supported in part by the Office of Fusion Energy, U.S. Department of Energy under Contract No. W-7405-ENG-26 with the Union Carbide Corporation.

[1]R. A. Falk, G. H. Dunn, D. C. Griffin, C. Bottcher, D. C. Gregory, D. H. Crandall, and M. S. Pindzola, Phys. Rev. Lett. 47, 494 (1981).

[2]*Photoionization and Other Probes of Many-Electron Interactions,* NATO/ASI/B18, edited by F. J. Wuilleumier (Plenum, New York, 1976).

[3]V. Pejcev, K. J. Ross, D. Rassi, and T. W. Ottley, J. Phys. B 10, 459 (1977).

[4]G. V. Marr and J. M. Austin, Proc. R. Soc. London A 310, 137 (1969).

[5]S. M. Younger, Phys. Rev. A 22, 2682 (1980).

[6]M. Wilson and M. Fred, J. Opt. Soc. Am. 59, 827 (1969).

[7]H. Li and K. L. Andrew, J. Opt. Soc. Am. 62, 1476 (1972).

[8]J. E. Hansen, J. Phys. B 5, 1083 (1972).

[9]R. L. Martin and P. J. Hay, J. Chem. Phys. 75, 4539 (1981).

[10]D. C. Gregory and D. H. Crandall, Phys. Rev. A 27, 2338 (1983) (subsequent paper).

[11]J. C. Slater, *Quantum Theory of Atomic Structure* (McGraw-Hill, New York, 1960), Vol. 1.

[12]C. F. Fischer, *The Hartree-Fock Method for Atoms* (Wiley, New York, 1977).

[13]C. F. Fischer, Comput. Phys. Commun. 14, 145 (1978).

[14]D. C. Griffin, K. L. Andrew, and R. D. Cowan, Phys. Rev. 177, 62 (1969).

[15]M. Mayer, Phys. Rev. 60, 184 (1941).

[16]W. A. Goddard, Phys. Rev. 174, 659 (1968).

[17]R. D. Cowan and D. C. Griffin, J. Opt. Soc. Am. 66, 1010 (1976).

[18]D. C. Griffin, C. Bottcher, and M. S. Pindzola, Phys. Rev. A 25, 154 (1982).

[19]J. H. Miller, R. L. Chase, A. W. Fliflet, G. R. Daum, S. L. Carter, and H. P. Kelly (unpublished).

[20]W. Lotz, Z. Phys. 216, 241 (1968); 220, 466 (1969).

[21]M. A. Crees, M. J. Seaton, and P. M. H. Wilson, Comput. Phys. Commun. 15, 23 (1978).

[22]S. M. Younger and W. L. Wiese, J. Quant. Spectrosc. Radiat. Transfer 22, 161 (1979).

[23]R. D. Cowan, *The Theory of Atomic Structure and Spectra* (University of California Press, Berkeley, 1981).

[24]M. E. Riley and D. G. Truhlar, J. Chem. Phys. 63, 2182 (1975).

[25]D. C. Gregory, P. F. Dittner, and D. H. Crandall, Phys. Rev. A 27, 762 (1983).

[26]G. Wendin, J. Phys. B 9, L297 (1976).